Yuan HX*, Wang YQ, Shi YJ, Gardner L. Residual stress distributions in welded stainless steel sections. Thin-Walled Structures, 2014(79): 38-51.

Residual stress distributions in welded stainless steel sections

H.X. Yuan[a,b,*], Y.Q. Wang[a], Y.J. Shi[a], L. Gardner[b]

[a]*Key Laboratory of Civil Engineering Safety and Durability of China Education Ministry, Department of Civil Engineering, Tsinghua University, Beijing 100084, PR China*

[b]*Department of Civil and Environmental Engineering, Imperial College London, London SW7 2AZ, United Kingdom*

Corresponding author: Dr Huanxin Yuan, School of Civil Engineering, Wuhan University, Wuhan 430072, China. Email: yuanhx@whu.edu.cn

Abstract

Residual stress magnitudes and distributions in structural stainless steel built-up sections have been comprehensively investigated in this study. A total of eighteen test specimens were fabricated from hot-rolled stainless steel plates by means of shielded metal arc welding (SMAW). Two grades of stainless steel were considered, namely the austenitic grade EN 1.4301 and the duplex grade EN 1.4462. Using the sectioning method, the test specimens were divided into strips. The residual stresses were then computed by multiplying the strains relieved during sectioning by the measured Young's moduli determined from tensile and compressive coupon tests. Residual stress distributions were obtained for ten I-sections, four square hollow sections (SHS) and four rectangular hollow sections (RHS). Peak tensile residual stresses reached around 80% and 60% of the material 0.2% proof stress for grades EN 1.4301 and EN 1.4462, respectively. Based upon the test data, simplified predictive models for residual stress distributions in stainless steel built-up I-sections and box sections were developed. Following comparisons with other available residual stress test data, the applicability of the proposed models was also extended to other stainless steel alloys. The proposed residual stress patterns are suitable for inclusion in future analytical models and numerical simulations of stainless steel built-up sections.

Keywords: Built-up section; Experiments; Predictive models; Residual stress; Sectioning method; Stainless steel; Welding

1. Introduction

Residual stresses in structural stainless steel sections may differ significantly from those in carbon steel sections, owing to distinct differences in material and thermal properties [1,2]. For cold-formed sections, residual stresses are mainly attributed to the coiling-uncoiling of the sheet material and to the press-braking or cold rolling operations [3,4], whereas in fabricated sections the localised welding heat input and uneven cooling are the key sources of residual stresses [5]. The residual stresses in structural sections can be determined by both destructive and non-destructive methods [6]. However, the non-destructive measuring techniques, such as X-ray diffraction, ultrasonic and magnetic methods, are often not practical for examining structural members. The sectioning method, due to its accuracy and simplicity, has been widely used to evaluate residual stresses in structural steel members. It was successfully used to determine residual stresses patterns in carbon steel sections [7], high strength steel sections [8] and cold-formed stainless steel sections [9]. This sectioning technique is based upon the measurement of residual strains that are relieved when cutting test sections into small strips [10].

Measurements of residual stress in structural stainless steel sections have been reported in a number of previous experimental programmes. Young and Lui [11] presented measurements in two cold-formed RHS by means of the sectioning method, whereas Jandera and Gardner [12] examined residual stresses in cold-rolled stainless steel box sections by X-ray diffraction. A comprehensive experimental programme carried out by Cruise and Gardner [9]

involved the measurement of residual stresses in hot-rolled and press braked stainless steel angles, as well as cold-rolled box sections, using the sectioning method. For fabricated structural stainless steel sections, residual stress measurements using the sectioning technique have been made on four I-sections by Bredenkamp et al. [13], two I-sections by Lagerqvist and Olsson [14] and six I-sections by Wang et al. [15]. Overall, with relatively few residual stress measurements on welded stainless steel I-sections and none on welded stainless steel hollow sections, coupled with an increasing use of stainless steel in heavier load-bearing applications, the focus of this study is to carry out comprehensive measurements on fabricated sections and to develop simplified models for predicting the magnitudes and distributions of their residual stresses.

A total of eighteen structural stainless steel built-up sections, including ten I-sections, four SHS and four RHS were examined to acquire the level and distribution of residual stresses present in such sections. The sectioning method, using the wire-cutting technique, was adopted in the experimental programme. Relieved strains from a total of 1244 strips were measured using a standard Whittemore gauge. The residual stress magnitudes and patterns were calculated by utilising the material properties obtained from the original plates used to fabricate the sections. Based on the acquired data, together with all previously available results, existing residual stress predictive models [16,17] for carbon steel built-up sections were revised to provide corresponding models for structural stainless steel built-up sections.

2. Test specimens: geometric dimensions, fabrication process and material properties

The basic geometries of the test specimens are shown in Fig. 1. The measured geometric dimensions of the specimens are recorded in Tables 1 and 2. The constitutive plates of all the specimens were cut using a water jet from hot-rolled coil, with the longitudinal direction of the members parallel to the coil rolling direction. The web plates of the SHS and RHS were machined to create beveled edges for butt welds. The specimens were initially assembled by spot welding, prior to the final fillet and butt welding for the I-sections, and hollow sections, respectively. All welds were performed by shielded metal arc welding (SMAW), also known as manual metal arc welding (MMA). The choice of electrodes was dependent on the parent material [18]. Specifically, type E308 electrodes were used for the grade EN 1.4301 specimens (corresponding to type 304 in the ASTM system), while type E2209 electrodes were selected for the grade EN 1.4462 specimens (corresponding to type 2205 in the ASTM system). The size of both the fillet welds and the butt welds was designed to be 5 mm, taking consideration of both strength and construction requirements.

The physical and thermal properties of the investigated stainless steel grades are such that welding distortions can be more significant than in equivalent carbon steel sections. In comparison to carbon steel, larger welding distortions can arise in stainless steel sections due to sharper heat gradients resulting from lower heat conductivity and a higher coefficient of thermal expansion. To alleviate the induced welding distortions, two techniques, namely reverse bending of the I-section flange plates before assembling and symmetric welding sequences, were introduced into the fabrication process. Subsequent to welding, additional straightening of the constitutive plates by means of a hydraulic press and a specially designed clamping apparatus was implemented. The eighteen welded test specimens are shown in Fig. 2.

The material properties were tested in a previous study [19], which unveiled both anisotropic and asymmetric features of the alloys. Since the test specimens were built up by plates all cut along the rolling direction, the corresponding tensile and compressive material properties are listed in Table 3, where the following symbols are used: E_0 is the Young's modulus, $\sigma_{0.01}$ and $\sigma_{0.2}$ are the 0.01% and 0.2% proof stresses, respectively, σ_u is the ultimate tensile stress, ε_f is the plastic strain at fracture, measured from the fractured tensile coupons as elongation over the standard gauge length, and n is the Ramberg-Osgood strain hardening exponent.

3. Measuring technique: the sectioning method

The sectioning method, which is a destructive technique for measuring residual stresses, has been widely used for many years and found to provide accurate and reliable results. This method was employed in the present study. The test specimens were designed to be sufficiently long to enable consistent and uniform welds to be established and to minimise end effects. The total length of each test specimen lay within the limits set by the Structural Stability Research Council [20], as illustrated in Fig. 3.

After inspecting the welds and measuring the geometric dimensions of the specimens, gauge holes were prepared in which to locate a standard Whittemore gauge. One pair of 2 mm diameter gauge holes was drilled in each designated strip over a gauge length of 254 mm (10 in.) using a bench drilling machine (Fig. 4 (a)). The nominal width of each strip was set as 10 mm. The total number of strips was 1244 with 2488 gauge holes. In order to remove any burrs from the drilling operations and enable better contact surfaces between the gauge holes and the Whittemore gauge, the gauge holes were chamfered to a depth of 0.5 mm. The completed set of gauge holes for one specimen is shown in Fig. 4 (b).

Gauge length readings were taken for each strip using the Whittemore gauge prior to and subsequent to the sectioning process. For the purpose of minimising the influence of temperature changes, a temperature reference bar was employed. The measured length of the reference bar was denoted as t_1. The initial readings of the specimens were taken after cleaning the gauge holes with an air blast. The mean value of three sets of repeated readings on each pair of gauge holes was recorded as the initial gauge length (denoted as r_1).

All cutting operations performed during the sectioning process of this experimental programme were conducted using an automated electric spark wire-cutting machine (Fig. 5), with minimal heat input brought into the test specimens. After extracting from the welded test specimens (as shown in Fig. 6) the test pieces were cut into their pre-designed strips. Fig. 7 presents two fully sectioned test specimens – I304-192 and S2205-130. After sectioning, the final gauge length readings (denoted as r_2) were taken for each of the strips, with the corresponding temperature reference bar readings recorded as t_2.

4. Measured residual stress magnitudes and distributions

4.1 Calculation of residual stresses

For each strip, both the exterior and interior readings were taken using the standard Whittemore gauge. By means of the temperature reference bar, corrections for any temperature changes were also made. The relieved residual strains were calculated as follows:

$$\varepsilon = \frac{(r_2 - t_2) - (r_1 - t_1)}{L_0 + r_1 - t_1} \tag{1}$$

in which L_0 is the gauge length and equal to 254 mm (10 in.). It should be noted that a negative relieved strain corresponds to a tensile residual stress, while a positive strain value indicates a compressive residual stress.

Strips with a significant stress gradient through the thickness, such as those near the welds, exhibited longitudinal curvature upon sectioning. The final readings over the gauge length were therefore chord lengths rather than arc lengths. This required chord to arc length corrections to be carried out using the offset value δ and the initial gauge length L, defined in Fig. 8. The true relieved strain, taking the curvature correction into consideration, can be approximated as [10]

$$\varepsilon_c = \varepsilon + \frac{(\delta/L)^2}{6(\delta/L)^4 + 1} \tag{2}$$

in which the δ/L is the ratio of the offset δ to the initial gauge length L. The curvature correction may be neglected until this ratio exceeds 0.001.

4.2 Obtained residual stress distribution patterns

The relieved residual strains were multiplied by either the tensile or compressive Young's modulus, depending on the direction of straining, to compute the corresponding residual stresses. The mean values of the exterior and interior residual stresses were calculated. The measured residual stresses and distribution patterns for the eighteen tested stainless steel built-up sections are plotted in Figs 9 and 10. The results may be seen to follow a consistent trend and to accord with the anticipated pattern of tensile residual stresses in the vicinity of the welds and compressive residual stresses remote from these regions.

5. Analysis of the results and development of simplified predictive models

5.1 General

In this section, the obtained residual stress measurements are used to establish a suitable predictive model for stainless steel built-up sections. The basic form of the predictive models followed that of the ECCS [16,17] and BSK 99 [21] models for carbon steel built-up sections, which is shown in Fig. 11. The tensile residual stresses are marked as positive while the compressive values are indicated as negative. Clearly, over the full cross-section, the residual stress distribution must be in self-equilibrium.

5.2 Summary of the test data

The peak residual stress values obtained from the tests are tabulated in Tables 4 and 5. The residual stresses are also presented in normalised form, with respect to the measured yield strengths. For each I-section specimen, there are four peak tensile stresses: one from each of the two flanges (σ_{ft}) and one from each of the two ends of the web (σ_{wt}), and five peak compressive stresses: four from the flange tips (σ_{fc}) and one from the middle of the web (σ_{wc}). As for the hollow sections, there are two peak tensile stresses (σ_{sft} or σ_{swt}) and one compressive stress (σ_{sfc} or σ_{swc}) in each constitutive plate, which means eight peak tensile stresses and four compressive stresses for a whole section.

The peak values of tensile and compressive residual stress were averaged for each section, separately, as listed in Tables 6 and 7. All the peak values of residual stresses are below the respective measured material yield strengths. The maximum values of tensile residual stresses in the grade EN 1.4301 sections reached $0.76\sigma_{0.2}$, while the maximum tensile residual stress in the grade EN 1.4462 sections was $0.55\sigma_{0.2}$. For the welded hollow sections, the maximum compressive residual stresses varied between sections depending on the width-to-thickness ratios of the elements.

5.3 Existing predictive models for residual stresses

For welded carbon steel sections, both the ECCS [16,17] and BSK 99 [21] provide models for predicting the residual stress distributions. The key parameters (as defined in Fig. 11) are detailed in Tables 8 and 9, underpinned by the basic assumption that each constitutive plate must be in self-equilibrium. The main difference between the models presented by ECCS and BSK 99 for the I-sections is in the definition of the key parameters, with the ECCS model based on the plate widths and the BSK 99 model based on the plate thicknesses. In both cases, the peak tensile residual stresses are taken as the material yield strength $\sigma_{0.2}$, and the compressive residual stresses can be calculated by complying with the equilibrium equations,

$$\sigma_{fc} = \frac{a+b}{b_f-(a+b)}\sigma_{ft}$$
$$\sigma_{wc} = \frac{2c+d}{h_w-(2c+d)}\sigma_{wt} \qquad \text{For I-sections} \qquad (3)$$

$$\sigma_{\mathrm{sfc}} = \frac{2e+f}{b_{\mathrm{f}} - (2e+f)}\sigma_{\mathrm{sft}}$$
$$\sigma_{\mathrm{swc}} = \frac{2g+h}{h_{\mathrm{w}} - (2g+h)}\sigma_{\mathrm{swt}} \qquad \text{For box sections} \qquad (4)$$

where the symbols are illustrated in Fig. 11.

The measured residual stress data is compared to the existing predictive models [16,17,21] for welded carbon steel sections in Figs. 12-15. As expected, the existing models do not represent accurately the obtained stainless steel residual stresses data, and the following observations can be made regarding the comparisons:

(1) The peak values of tensile residual stresses are markedly lower than the material yield strength, yet the acquired compressive residual stresses display higher values than expected. Gardner and Cruise [22] had suggested that peak tensile residual stresses in stainless steel fabricated I-sections could be greater than $\sigma_{0.2}$, though this was on a characteristic basis (i.e. 5% probability of exceedance) and a limited pool of test data. Mean values of peak tensile residual stresses were found to be generally similar to those measured herein and were less than $\sigma_{0.2}$. The lower peak tensile residual stresses could be attributed to the fact that higher strains are required to reach the equivalent yield stress (i.e. $\sigma_{0.2}$) in materials with rounded stress-strain curves than to reach the distinct yield point of conventional structural steels. Furthermore, less heat input may be required during the welding process of stainless steel sections than carbon steel sections, since fusion of the stainless steel weld regions can be more easily achieved due to its higher electrical resistance [23].

(2) The regions of peak tensile residual stresses in welded stainless steel sections tend to be narrower than in carbon steel sections, yet the transition regions appear to be much wider. This can be attributed to the lower thermal diffusivity of stainless steel, which can result in slower cooling and hence a wider heat affected zone, slower heat diffusion through the base metal means the weld region remain hot longer, producing wider transition zones [24,25].

(3) Finally, examination of the test data suggests that flange width rather than flange thickness is more influential on the size of the peak tensile residual stress region. This may be illustrated by considering, for example, specimens I2205-192 and I2205-200, which have the same web height and flange width, but despite different flange thicknesses, exhibit similar tensile residual stress regions in the flanges. This observation suggests that the ECCS predictive model, where the size of the tensile residual stress zones is dependent on the flange width, will serve as a suitable basis for welded stainless steel I-sections.

5.4 Proposed distribution models

Following analysis of the test data obtained in this study and all other available test results for structural stainless steel built-up sections [13-15], it is revealed that all collected tensile residual stress peak values are lower than the corresponding yield strengths except one single value ($1.18\sigma_{0.2}$) reported by Lagerqvist and Olsson [14]. Overall, it is proposed that the peak value of tensile stresses in stainless steel built-up sections can be approximated by Eq. (5).

$$\sigma_{\mathrm{ft}} = \sigma_{\mathrm{wt}} = \begin{cases} 0.8\sigma_{0.2} & \text{For austenitic alloys} \\ 0.6\sigma_{0.2} & \text{For duplex and ferritic alloys} \end{cases} \qquad (5)$$

Owing to the mechanical and thermal similarities among families of stainless steel alloys, the results obtained for grades EN 1.4301 and EN 1.4462 may be generalised to austenitic alloys and duplex (and also ferritic) alloys respectively; broadening this will be verified in the next sub-section. In view of the lower peak tensile residual stresses but wider tension zones observed from the tests, the existing predictive models will now be revised to adapt to the test data points. The key related parameters for predicting residual stress distributions in stainless steel built-up sections are proposed in Tables 10 and 11 for I-sections and box sections, respectively. The distribution

parameters for welded I-sections made of different alloys are the same except for the stress amplitudes. The key parameters for welded box sections depend on the plate width-to-thickness ratios with the demarcation ratio taken as 20.

The proposed predictive models are compared with the test results in Figs. 16-19. In the normalised residual stress versus position figures, the proposed models for I-sections can be plotted as the unified line, whereas for box sections the distribution patterns vary between specimens. Specifically, for box sections with a plate slenderness ratio h/t or $b_f/t<20$, the width of the peak tension region reduces to zero. It can be seen that the proposed models provide accurate predictions for residual stresses in stainless steel built-up sections of grades EN 1.4301 and EN 1.4462.

5.5 Validation of the proposed models with other available test data

Other existing residual stress test data from welded stainless steel sections are gathered and used to validate further the proposed predictive models in this sub-section. Two welded I-sections, of grades EN 1.4301 and EN 1.4462, were examined by Lagerqvist and Olsson [14] to assess their residual stress state. With reference to Fig. 20, good predictions of the measured residual stress distributions are offered by the proposed models.

Wang et al. [15] measured residual stresses in six welded I-sections of austenitic alloy EN 1.4401 (AISI 316), which were fabricated by tungsten inert gas welding. The constitutive plates were directly cut from cold-rolled coil using a guillotine shear machine. The predictions from the proposed models for these six sections are presented in Fig. 21. It can be observed that the predicted residual stress values are close to the measured results, which supports the extension of the proposed models to other austenitic alloys.

Residual stresses in four fabricated I-sections of grade EN 1.4003 (AISI 409) ferritic stainless steel were experimentally determined by Bredenkamp et al. [13]. Fig. 22 compares the predicted distributions and the test data points. In view of the satisfactory agreement, it can be concluded that the proposed models could be successfully extended to ferritic alloys.

The mean values of residual stress prediction ratios (Predicted/Test) and the corresponding coefficient of variation (COV) are summarised for all the available test data in Table 12. The comparison has involved thirty welded stainless steel I-sections and box sections, with two austenitic grades, one duplex grade and one ferritic grade incorporated. The mean Predicted/Test ratios are generally close to unity, confirming the accuracy of the proposed predictive models. Certain scatter of the residual stress predictions can also be observed, which may be attributed to the inherent scatter of the test data.

In summary, the proposed models for predicting magnitudes and distributions of residual stresses in welded stainless steel sections accord well with available test data. The supplementary verifications allow the proposed models to be extended to other stainless steel alloys, and cover the three broad families of austenitic, duplex and ferritic stainless steels.

6. Conclusions

Eighteen built-up stainless steel I-sections and box sections were fabricated and subsequently tested using the sectioning method to obtain the level and distribution of residual stresses. The test specimens were fabricated from hot-rolled stainless steel plates, welded together by means of shielded metal arc welding (SMAW). A total of 1244 residual stress measurements were taken.

Comparing the obtained test data points with existing (ECCS and BSK 99) predictive models for residual stresses in welded carbon steel sections, it was found that the peak tensile residual stress values in the test specimens were lower than the material yield strength, and typically reached 60% - 80% of this value. The lower peak tensile residual stress values in welded stainless steel sections are attributed to both higher strains required to reach the equivalent yield stress with rounded stress-strain curves and less heat input during the welding process

due to higher electrical resistance compared with carbon steel sections. Furthermore, owing to the lower thermal diffusivity of stainless steel, the peak tension regions in welded stainless steel sections tend to be narrower than in carbon steel sections, yet the transition regions are wider.

Based upon the existing distribution patterns for residual stresses in welded carbon steel sections, new predictive models for determining the residual stresses in welded stainless steel I-sections and box sections were proposed, covering austenitic, duplex and ferritic alloys. The proposed models were not only validated against the test data obtained in this study, but also verified by all the other collected stainless steel residual stress test results. The proposed models are considered suitable for inclusion in analytical and numerical models and for underpinning code developments.

Acknowledgements

The authors would like to express their gratitude to the Specialised Research Fund for the Doctoral Program of Higher Education (No.20110002130002) and Beijing Natural Science Foundation (No.8112018) for their financial support. The first author also appreciates the financial support from the State Scholarship Fund for sponsoring studying abroad, Academic Scholarship for Doctoral Candidates awarded by Ministry of Education of the P.R. China (2012), and Ng Teng Fong/Sino Support Fund for Doctoral Candidates.

References

[1] Gardner L, Ng KT. Temperature development in structural stainless steel sections exposed to fire. Fire Safety Journal, 2006(41): 185-203.
[2] Huang Y, Young B. Material properties of cold-formed lean duplex stainless steel sections. Thin-Walled Structures, 2012(54): 72-81.
[3] Quach WM, Teng JG, Chung KF. Residual stresses in press-braked stainless steel sections, I: Coiling and uncoiling of sheets. Journal of Constructional Steel Research, 2009(65): 1803-1815.
[4] Quach WM, Teng JG, Chung KF. Residual stresses in press-braked stainless steel sections, II: Press-braking operations. Journal of Constructional Steel Research, 2009(65): 1816-1826.
[5] Withers PJ, Bhadeshia HKDH. Residual stress. Part 2 – Nature and origins. Materials Science and Technology, 2001(17): 366-375.
[6] Withers PJ, Turskia M, Edwards L, Bouchard PJ, Buttle DJ. Recent advances in residual stress measurement. International Journal of Pressure Vessels and Piping, 2008(85): 118-127.
[7] Huber AW, Beedle LS. Residual stress and the compressive strength of steel. Welding Journal, 1954(33): 589-614.
[8] Rasmussen KJR, Hancock GJ. Plate slenderness limits for high strength steel sections. Journal of Constructional Steel Research, 1992(23): 73-96.
[9] Cruise RB, Gardner L. Residual stress analysis of structural stainless steel sections. Journal of Constructional Steel Research, 2008(64): 352-366.
[10] Tebedge N, Alpsten G, Tall L. Residual-stress measurement by the sectioning method. Experimental Mechanics, 1973; 13(2): 88-96.
[11] Young B, Lui WM. Behavior of cold-formed high strength stainless steel sections. Journal of Structural Engineering, ASCE, 2005, 131(11): 1738-1745.
[12] Jandera M, Gardner L, Machacek J. Residual stresses in cold-rolled stainless steel hollow sections. Journal of Constructional Steel Research, 2008(64): 1255-1263.
[13] Bredenkamp PJ, van den Berg G J, van der Merwe P. Residual stresses and the strength of stainless steel I-section columns. Proc., Structural Stability Research Council, Annual Technical Session, 1992: 69-86.
[14] Lagerqvist O, Olsson A. Residual stresses in welded I-girders made of stainless steel and structural steel. Proc., 9th Nordic Steel Construction Conf., 2001: 737-744.
[15] Wang YQ, Guan J, Zhang Y, Shi YJ, Yang L. Experimental study on residual stress of austenitic stainless steel 316 in fabricated I-sections. Industrial Construction, 2012, 42(5): 44-50. [in Chinese]
[16] European Convention for Constructional Steelwork, ECCS. Ultimate limit state calculation of sway frames with rigid joints. Technical Committee 8 – Structural Stability Technical Working Group 8.2 – System. Publication no. 33, 1984.
[17] European Convention for Constructional Steelworks, ECCS. Manual on stability of steel structures – Part 2.2 Mechanical properties and residual stresses. 2nd Edition, Bruxelles: ECCS Publ., 1976.
[18] GB/T 983-1995. Stainless steel covered electrodes. Beijing: Standards Press of China, 1995. [in Chinese]
[19] Yuan HX, Wang YQ, Shi YJ, Gardner L. Stub column tests on stainless steel built-up sections. Thin-Walled Structures, Special Issue for Experts Seminar, 2013. [submitted]
[20] Ziemian RD. Guide to stability design criteria for metal structures. 6th ed.. New York: John Wiley & Sons, Inc., 2010.
[21] BSK 99. Swedish regulations for steel structures. Sweden: Boverket, Karlskrona, 2003.
[22] Gardner L, Cruise RB. Modeling of residual stresses in structural stainless steel sections. Journal of Structural Engineering,

ASCE, 2009, 135(1): 42-53.
[23] American Iron and Steel Institute, AISI. Welding of Stainless Steels and Other Joining Methods. Toronto: Nickel Development Institute, 1988.
[24] Weman K. Welding processes handbook. Cambridge: Woodhead Publishing Ltd, 2003.
[25] Armentani E, Esposito R, Sepe R. The effect of thermal properties and weld efficiency on residual stresses in welding. Journal of Achievements in Materials and Manufacturing Engineering, 2007, 20(1-2): 319-322.

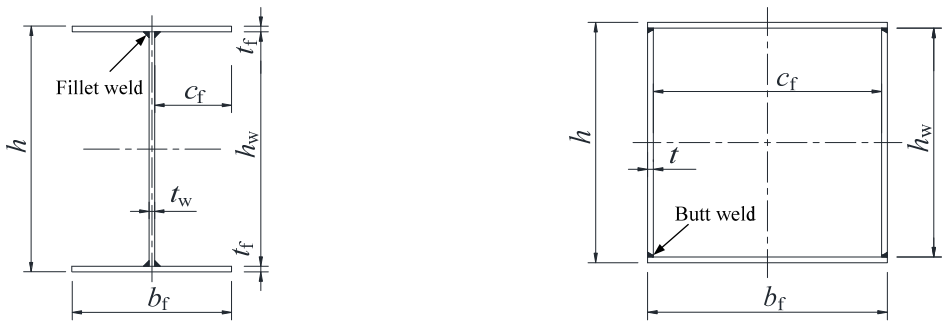

(a) I-section (b) SHS or RHS

Fig. 1. Definition of symbols and weld locations for the specimens

Fig. 2. Welded test specimens

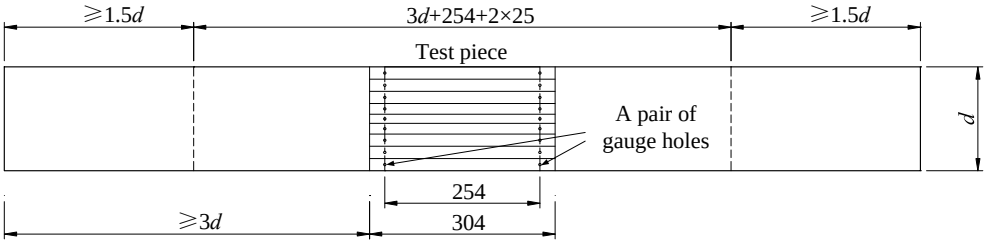

Fig. 3. Layout of the test pieces (dimensions in mm)

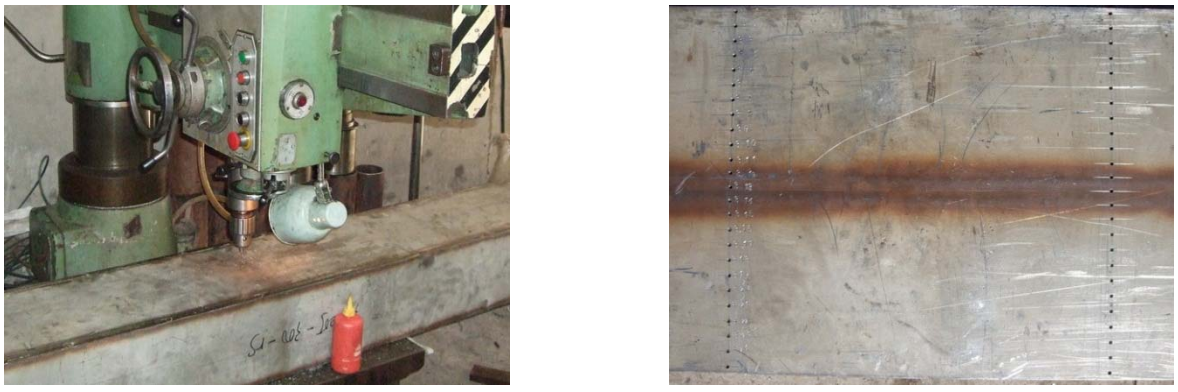

(a) Drilling process (b) Gauge holes

Fig. 4. Preparation of the gauge holes

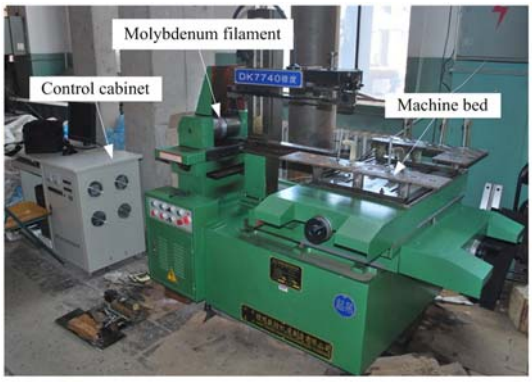

Fig. 5. Electric spark wire-cutting machine

Fig. 6. Extraction of the test pieces

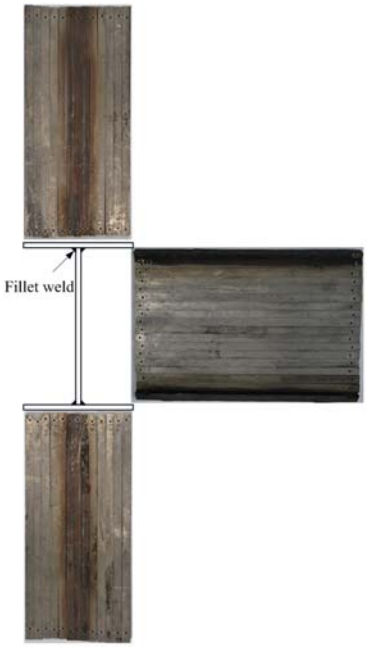

(a) I304-192

(b) S2205-130

Fig. 7. Sliced residual stress test pieces

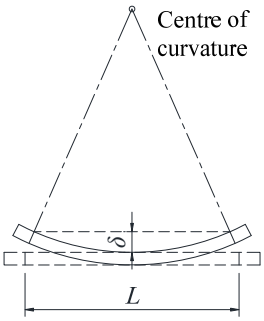

Fig. 8. Longitudinal curvature of strips and definition of curvature offset value δ

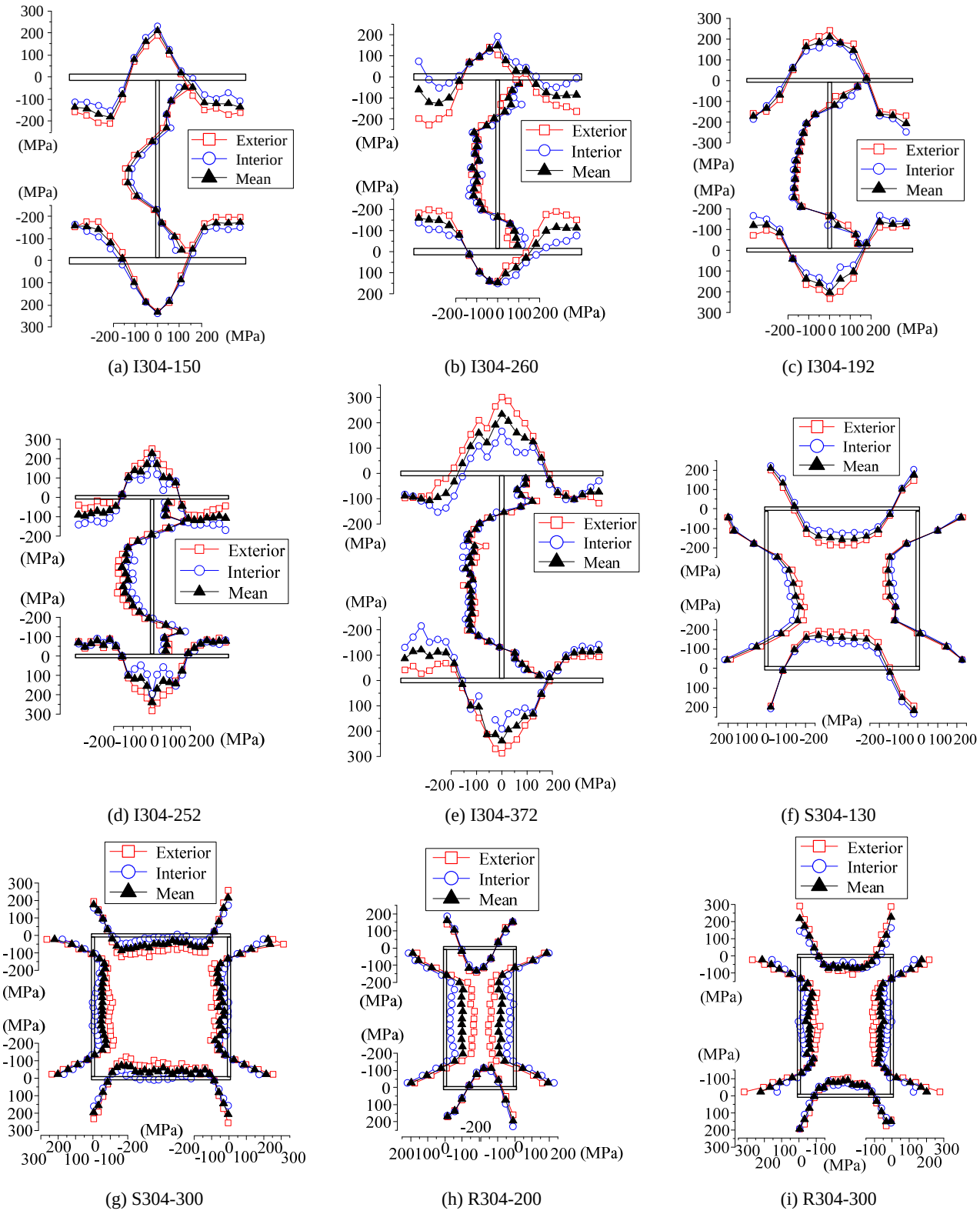

Fig. 9. Residual stress distributions in welded stainless steel sections of alloy EN 1.4301

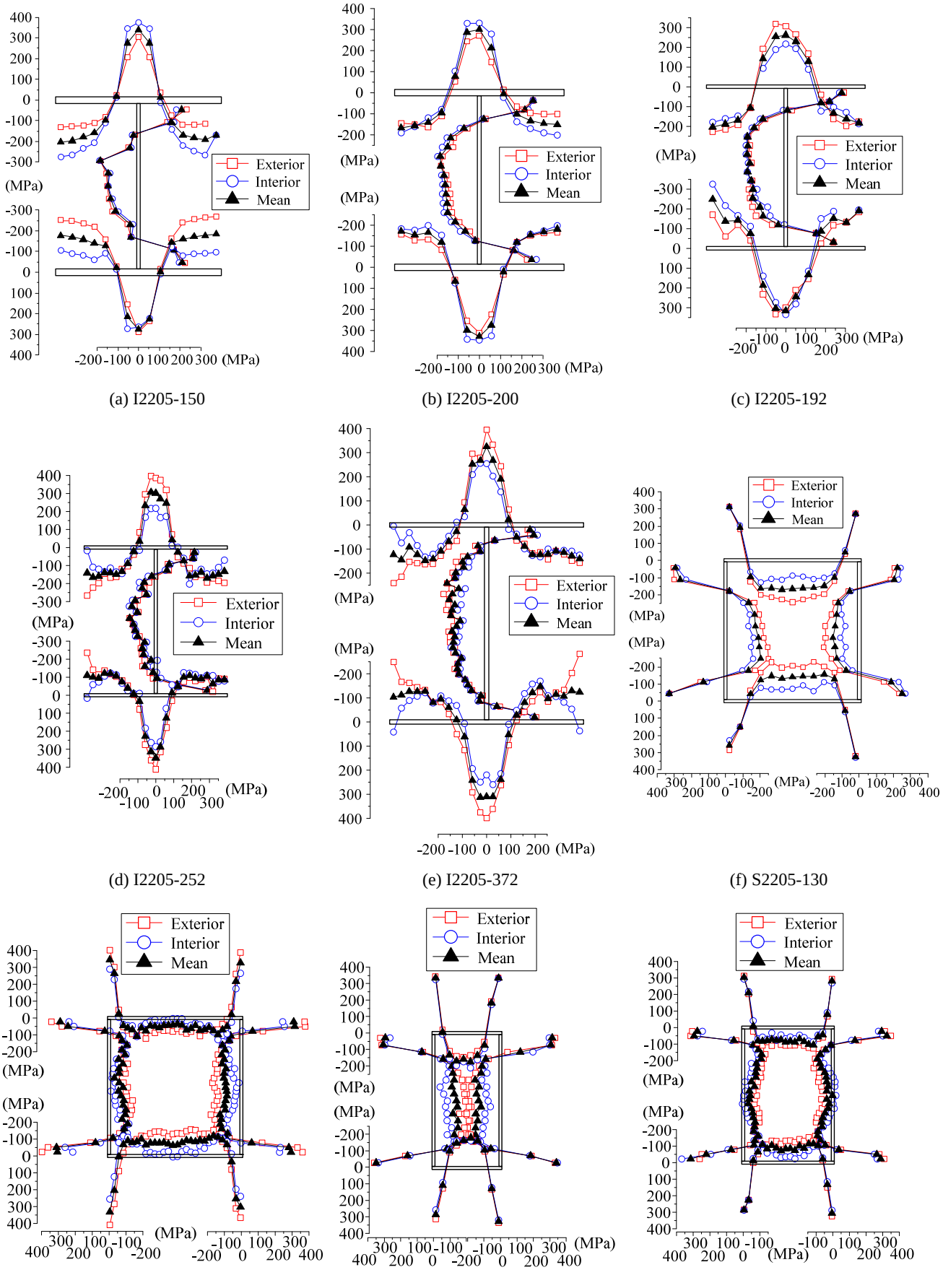

(a) I2205-150 (b) I2205-200 (c) I2205-192

(d) I2205-252 (e) I2205-372 (f) S2205-130

(g) S2205-300 (h) R2205-200 (i) R2205-300

Fig. 10. Residual stress distributions in welded stainless steel sections of alloy EN 1.4462

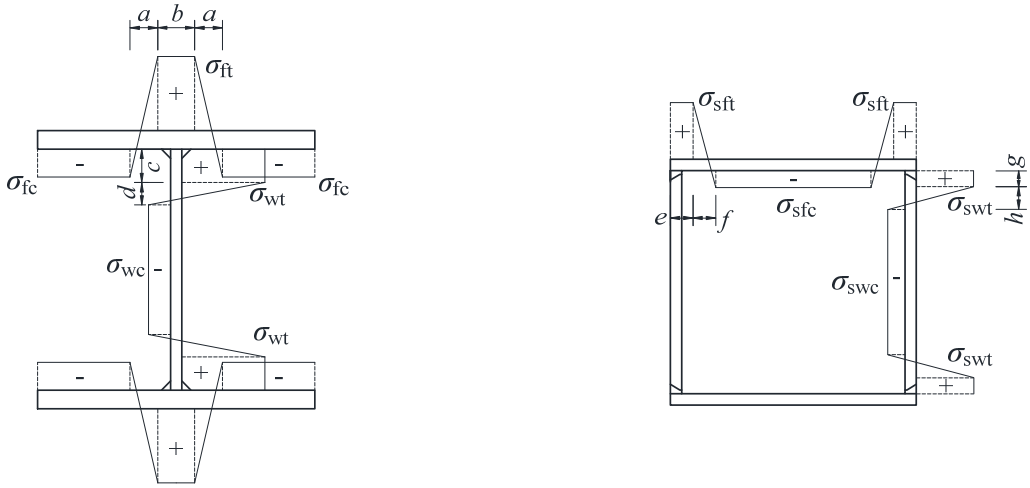

(a) I-section (b) Box sections (SHS or RHS)

Fig. 11. General residual stress distributions from ECCS and BSK models for carbon steel, used as basis for stainless steel predictive models

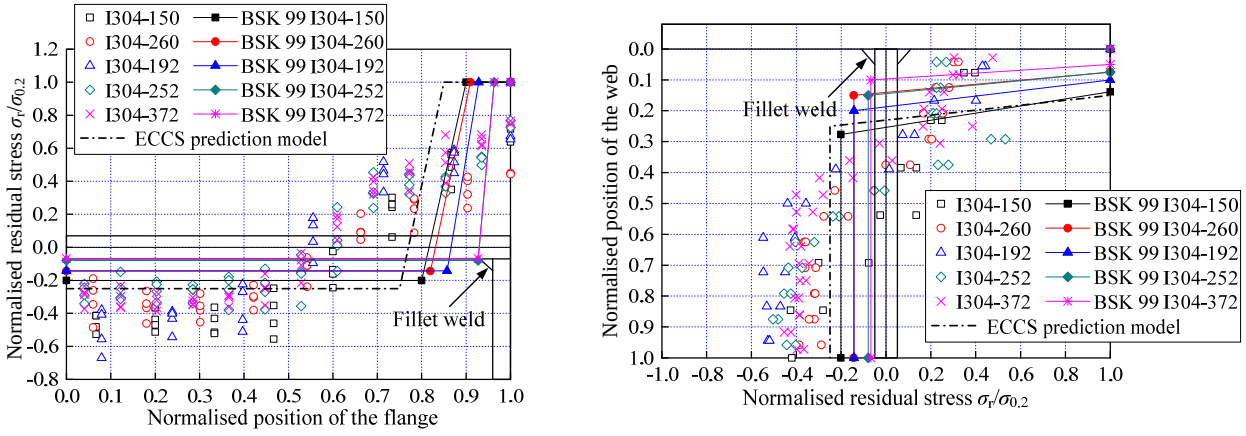

(a) Flange (b) Web

Fig. 12. Comparison between the test results and predictions from BSK 99 and ECCS models for EN 1.4301 I-sections

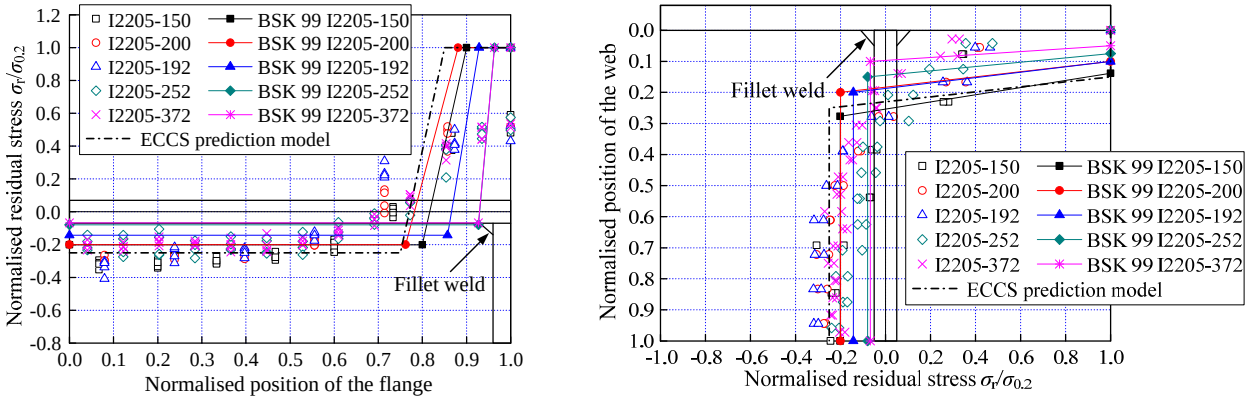

(a) Flange (b) Web

Fig. 13. Comparison between the test results and predictions from BSK 99 and ECCS models for EN 1.4462 I-sections

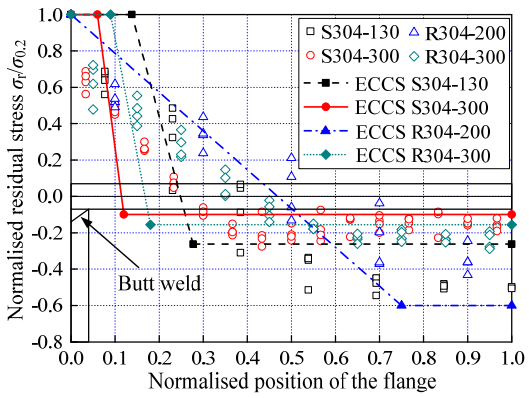

(a) Flange

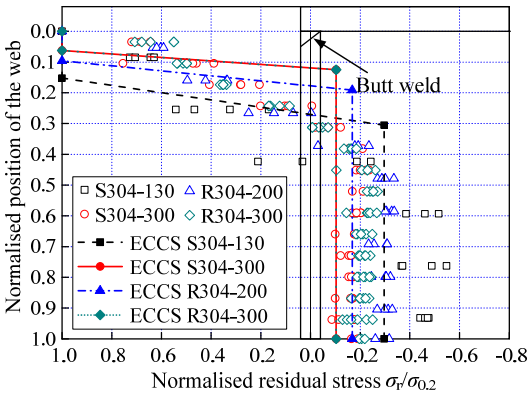

(b) Web

Fig. 14. Comparison between the test results and predictions from ECCS models for EN 1.4301 box sections

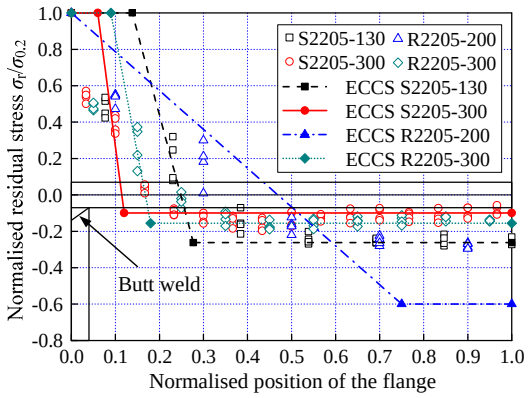

(a) Flange

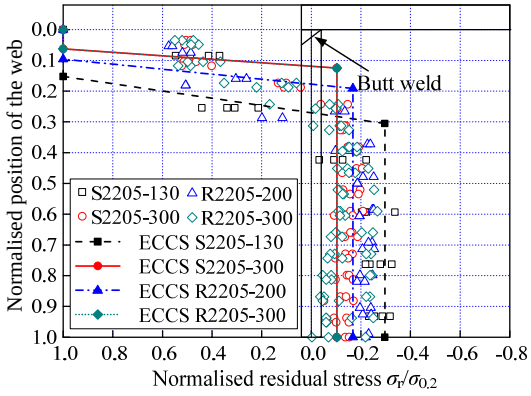

(b) Web

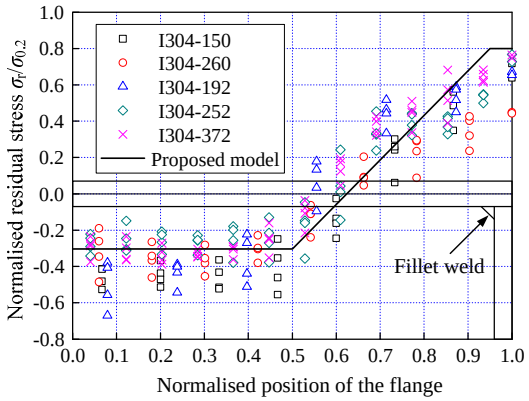

(a) Flange

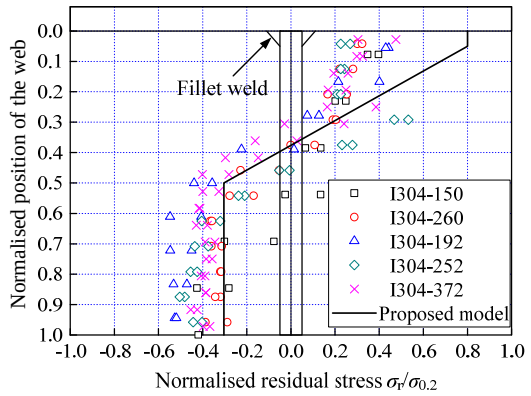

(b) Web

Fig. 16. Comparison of tested residual stresses with predictions from the proposed model for EN 1.4301 I-sections

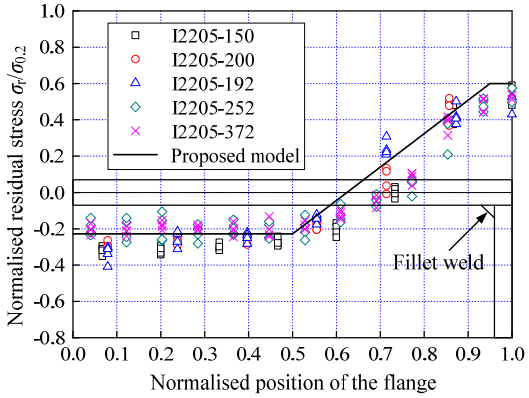

(a) Flange

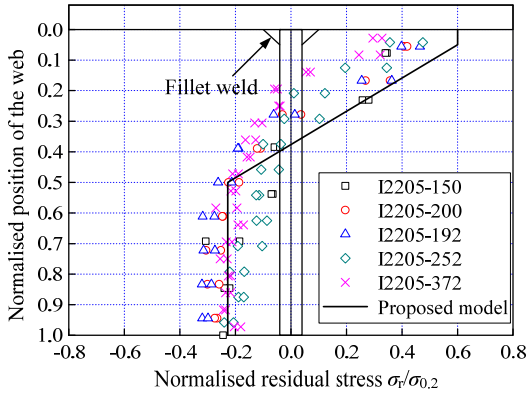

(b) Web

Fig. 17. Comparison of tested residual stresses with predictions from the proposed model for EN 1.4462 I-sections

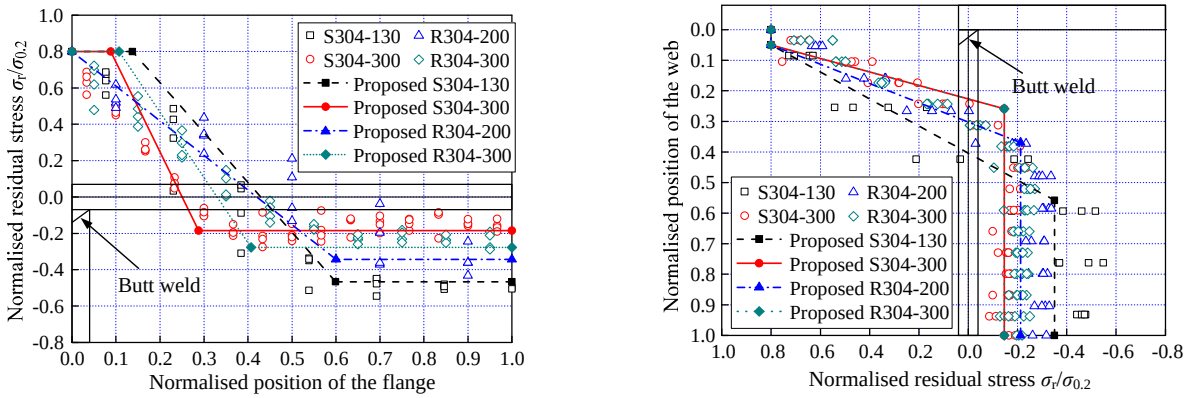

(a) Flange (b) Web

Fig. 18. Comparison of tested residual stresses with predictions from the proposed model for EN 1.4301 box sections

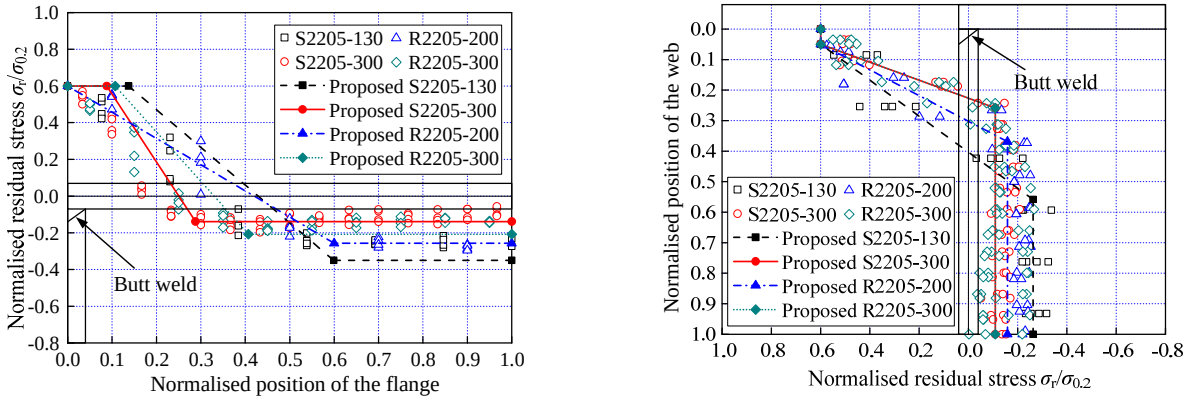

(a) Flange (b) Web

Fig. 19. Comparison of tested residual stresses with predictions from the proposed model for EN 1.4462 box sections

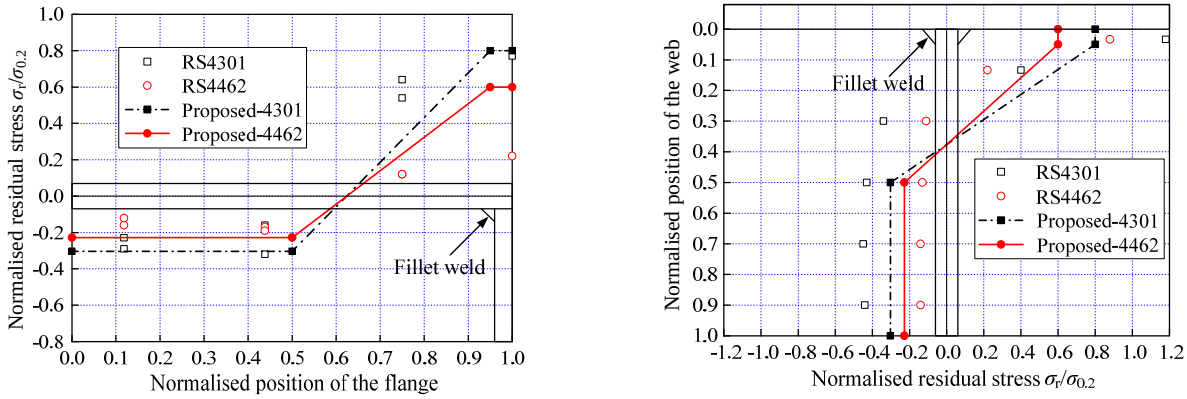

(a) Flange (b) Web

Fig. 20. Comparison of residual stresses in austenitic and duplex stainless steel sections from Lagerqvist and Olsson [14] with predictions from the proposed models

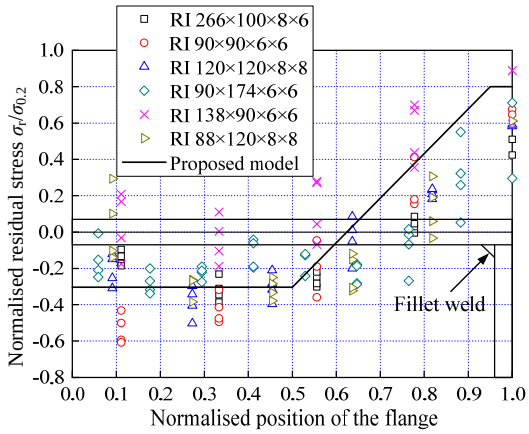

(a) Flange

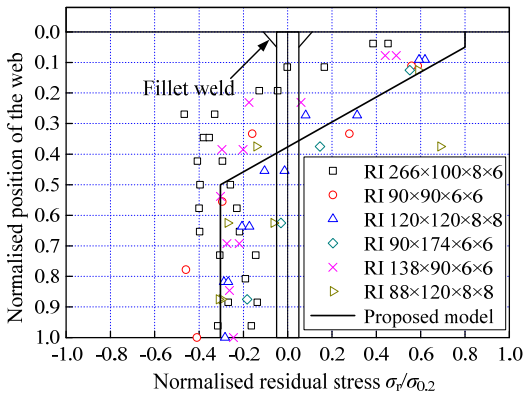

(b) Web

Fig. 21. Comparison of residual stresses in austenitic stainless steel sections from Wang et al. [15] with predictions from the proposed models

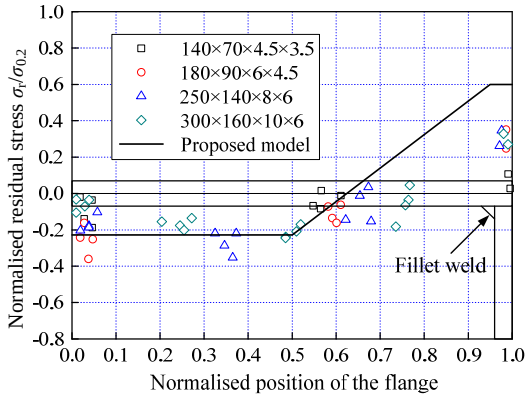

(a) Flange

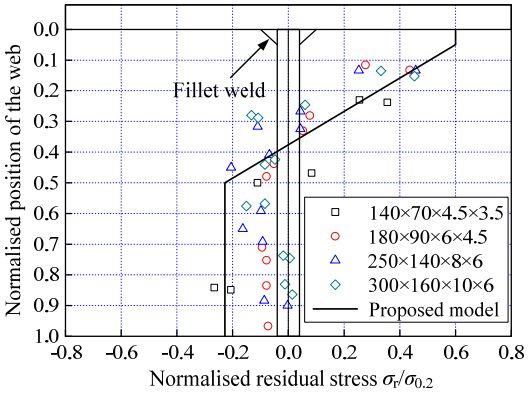

(b) Web

Fig. 22. Comparison of residual stresses in ferritic stainless steel sections from Bredenkamp et al. [13]with predictions from the proposed models

Table 1

Average measured geometric dimensions for I-section specimens

Specimen	b_f (mm)	h (mm)	t_w (mm)	t_f (mm)	c_f/t_f	h_w/t_w
I304-150	149.5	149.6	6.00	10.00	7.2	21.6
I304-260	165.7	259.0	6.00	10.00	8.0	39.8
I304-192	126.3	194.2	6.00	6.00	10.0	30.4
I304-252	245.7	253.3	6.00	6.00	20.0	40.2
I304-372	246.1	373.3	6.00	6.00	20.0	60.2
I2205-150	150.0	150.7	6.00	10.20	7.1	21.7
I2205-200	124.9	200.6	6.00	10.20	5.8	30.0
I2205-192	125.8	193.1	6.00	6.00	10.0	30.2
I2205-252	245.3	252.9	6.00	6.00	19.9	40.1
I2205-372	245.0	372.9	6.00	6.00	19.9	60.1

Table 2

Average measured geometric dimensions for RHS and SHS specimens

Specimen	b_f (mm)	h (mm)	t_w=t_f=t (mm)	c_f/t	h_w/t
R304-200	100.4	199.9	6.00	16.7	33.3
R304-300	200.1	299.7	6.00	33.3	50.0
S304-130	130.3	129.8	6.00	21.7	21.6
S304-300	301.3	300.7	6.00	50.2	50.1
R2205-200	100.4	200.1	6.00	16.7	33.4
R2205-300	200.9	300.6	6.00	33.5	50.1
S2205-130	130.5	130.3	6.00	21.8	21.7
S2205-300	299.9	301.0	6.00	50.0	50.2

Table 3

Measured material properties from tensile and compressive coupon tests

Grade	t (mm)	Direction	E_0 (MPa)	$\sigma_{0.01}$ (MPa)	$\sigma_{0.2}$ (MPa)	σ_u (MPa)	ε_f (%)	n
1.4301	6.00	LT	188600	186.3	312.6	695.7	60.6	5.8
		LC	182300	177.2	281.5	-	-	6.5
1.4301	10.00	LT	188800	213.0	328.5	659.8	55.5	6.9
		LC	198700	195.1	320.5	-	-	6.0
1.4462	6.00	LT	193200	404.4	605.6	797.9	34.6	7.4
		LC	191900	360.6	553.0	-	-	7.0
1.4462	10.20	LT	191200	366.8	574.8	775.0	35.4	6.7
		LC	190400	342.5	546.9	-	-	6.4

LT: Longitudinal Tension, LC: Longitudinal Compression.

Table 4

Peak residual stress values in welded stainless steel I-sections

Specimen	σ_{ft}(+)(MPa)	$\sigma_{ft}/\sigma_{f0.2}$	σ_{fc}(-)(MPa)	$\sigma_{fc}/\sigma_{f0.2}$	σ_{wt}(+)(MPa)	$\sigma_{wt}/\sigma_{w0.2}$	σ_{wc}(-)(MPa)	$\sigma_{wc}/\sigma_{w0.2}$
I304-150	209.6	0.64	-182.6	-0.57	124.2	0.40	-133.1	-0.47
			-136.1	-0.42				
	235.4	0.72	-158.2	-0.49	108.7	0.35		
			-173.2	-0.54				
I304-260	147.5	0.45	-125.7	-0.39	100.9	0.32	-120.9	-0.43
			-92.3	-0.29				
	145.6	0.44	-116.6	-0.36	94.0	0.30		
			-159.5	-0.50				
I304-192	210.2	0.67	-173.8	-0.62	134.4	0.43	-171.2	-0.61
			-209.4	-0.74				
	204.6	0.65	-137.3	-0.49	138.6	0.44		
			-121.4	-0.43				
I304-252	227.2	0.73	-95.6	-0.34	166.3	0.53	-157.7	-0.56
			-118.6	-0.42				
	239.9	0.77	-79.3	-0.28	146.3	0.47		
			-84.4	-0.30				
I304-372	233.7	0.75	-107.5	-0.38	120.6	0.39	-141.8	-0.50
			-102.0	-0.36				
	239.1	0.76	-117.0	-0.42	148.7	0.48		
			-121.0	-0.43				
I2205-150	339.6	0.59	-202.6	-0.37	206.3	0.34	-185.4	-0.34
			-191.5	-0.35				
	276.5	0.48	-183.1	-0.33	209.7	0.35		
			-177.9	-0.33				
I2205-200	299.7	0.52	-168.4	-0.31	253.8	0.42	-185.3	-0.34
			-151.7	-0.28				
	328.7	0.57	-181.8	-0.33	246.7	0.41		
			-170.4	-0.31				
I2205-192	260.9	0.43	-204.7	-0.37	281.5	0.46	-193.8	-0.35
			-182.7	-0.33				
	317.5	0.52	-188.3	-0.34	240.9	0.40		
			-247.3	-0.45				
I2205-252	306.7	0.51	-166.2	-0.30	215.8	0.36	-145.4	-0.26
			-170.5	-0.31				
	348.6	0.58	-108.7	-0.20	287.6	0.47		
			-121.6	-0.22				
I2205-372	324.6	0.54	-148.3	-0.27	194.6	0.32	-163.5	-0.30
			-141.3	-0.26				
	313.2	0.52	-146.7	-0.27	198.3	0.33		
			-127.0	-0.23				

Table 5

Peak residual stress values in welded stainless steel hollow sections

Specimen	σ_{sft}(+)(MPa)		$\sigma_{sft}/\sigma_{0.2}$		σ_{sfc}(-)(MPa)	$\sigma_{sfc}/\sigma_{0.2}$	σ_{swt}(+)(MPa)		$\sigma_{swt}/\sigma_{0.2}$		σ_{swc}(-)(MPa)	$\sigma_{swc}/\sigma_{0.2}$
S304-130	210.6	175.1	0.67	0.56	-155.5	-0.55	220.6	227.4	0.71	0.73	-152.7	-0.54
	214.5	199.7	0.69	0.64	-170.5	-0.61	201.4	196.8	0.64	0.63	-171.2	-0.61
S304-300	175.9	214.9	0.56	0.69	-86.1	-0.31	236.0	213.5	0.75	0.68	-80.0	-0.28
	206.6	196.6	0.66	0.63	-72.4	-0.26	201.6	220.7	0.64	0.71	-73.8	-0.26
R304-200	162.5	153.2	0.52	0.49	-135.0	-0.48	185.0	193.6	0.59	0.62	-95.6	-0.34
	193.0	167.7	0.62	0.54	-113.2	-0.40	198.2	188.7	0.63	0.60	-105.5	-0.37
R304-300	217.9	225.8	0.70	0.72	-73.9	-0.26	171.9	201.3	0.55	0.64	-81.7	-0.29
	151.5	193.5	0.48	0.62	-90.2	-0.32	221.0	212.4	0.71	0.68	-84.4	-0.30
S2205-130	311.8	271.1	0.51	0.45	-169.9	-0.31	223.7	250.7	0.37	0.41	-153.9	-0.28
	323.9	255.9	0.53	0.42	-156.3	-0.28	330.7	294.7	0.55	0.49	-204.2	-0.37
S2205-300	345.3	326.0	0.57	0.54	-109.2	-0.20	316.1	293.9	0.52	0.49	-126.2	-0.23
	302.9	332.5	0.50	0.55	-119.8	-0.22	310.7	289.2	0.51	0.48	-110.3	-0.20
R2205-200	333.5	333.2	0.55	0.55	-174.1	-0.31	314.3	339.1	0.52	0.56	-153.7	-0.28
	327.7	286.2	0.54	0.47	-178.7	-0.32	348.3	306.0	0.58	0.51	-149.0	-0.27
R2205-300	302.9	281.4	0.50	0.46	-106.4	-0.19	324.7	287.8	0.54	0.48	-92.4	-0.17
	306.1	286.3	0.51	0.47	-114.6	-0.21	315.1	295.0	0.52	0.49	-110.5	-0.20

Table 6

Summary of the obtained peak residual stresses from welded stainless steel I-sections

Specimen	$\sigma_{ft}/\sigma_{0.2}$	$\sigma_{fw}/\sigma_{0.2}$	$\sigma_{fc}/\sigma_{0.2}$	$\sigma_{wc}/\sigma_{0.2}$	Specimen	$\sigma_{ft}/\sigma_{0.2}$	$\sigma_{fw}/\sigma_{0.2}$	$\sigma_{fc}/\sigma_{0.2}$	$\sigma_{wc}/\sigma_{0.2}$
I304-150	0.68	0.37	-0.51	-0.47	I2205-150	0.54	0.34	-0.35	-0.34
I304-260	0.45	0.31	-0.39	-0.43	I2205-200	0.55	0.41	-0.31	-0.34
I304-192	0.66	0.44	-0.57	-0.61	I2205-192	0.48	0.43	-0.37	-0.35
I304-252	0.75	0.50	-0.34	-0.56	I2205-252	0.54	0.42	-0.26	-0.26
I304-372	0.76	0.43	-0.40	-0.50	I2205-372	0.53	0.32	-0.25	-0.30
Mean	**0.66**	**0.41**	**-0.44**	**-0.51**	**Mean**	**0.53**	**0.39**	**-0.31**	**-0.32**
Maximum	**0.76**	**0.50**	**-0.57**	**-0.61**	**Maximum**	**0.55**	**0.43**	**-0.37**	**-0.35**

Table 7

Summary of the obtained peak residual stresses from welded stainless steel hollow sections

Specimen	$\sigma_{ft}/\sigma_{0.2}$	$\sigma_{fw}/\sigma_{0.2}$	$\sigma_{fc}/\sigma_{0.2}$	$\sigma_{wc}/\sigma_{0.2}$	Specimen	$\sigma_{ft}/\sigma_{0.2}$	$\sigma_{fw}/\sigma_{0.2}$	$\sigma_{fc}/\sigma_{0.2}$	$\sigma_{wc}/\sigma_{0.2}$
S304-130	0.64	0.68	-0.58	-0.58	S2205-130	0.48	0.45	-0.29	-0.32
S304-300	0.63	0.70	-0.28	-0.27	S2205-300	0.54	0.50	-0.21	-0.21
R304-200	0.54	0.61	-0.44	-0.36	R2205-200	0.53	0.54	-0.32	-0.27
R304-300	0.63	0.65	-0.29	-0.30	R2205-300	0.49	0.50	-0.20	-0.18
Mean	**0.61**	**0.66**	-	-	**Mean**	**0.51**	**0.50**	-	-
Maximum	**0.64**	**0.70**	**-0.58**	**-0.58**	**Maximum**	**0.54**	**0.54**	**-0.32**	**-0.32**

Table 8

Parameters in the predictive models for residual stresses in carbon steel built-up I-sections

	$\sigma_{ft}=\sigma_{wt}$	$\sigma_{fc}=\sigma_{wc}$	a	b	c	d
ECCS	$\sigma_{0.2}$	$0.25\sigma_{0.2}$	$0.05b_f$	$0.15b_f$	$0.075h_w$	$0.05h_w$
BSK 99	$\sigma_{0.2}$	From Eq. (3)	$0.75t_f$	$1.5t_f$	$1.5t_w$	$1.5t_w$

Table 9

Parameters in the predictive models for residual stresses in carbon steel built-up box sections

Ratio	Type of weld	σ_{sft}	σ_{sfc}	e	f
h/t=10	-	$\sigma_{0.2}$	$0.6\sigma_{0.2}$	0	From Eq. (4)
$h/t\geq$20	Heavy weld	$\sigma_{0.2}$	From Eq. (4)	3t	3t
	Light weld	$\sigma_{0.2}$	From Eq. (4)	1.5t	1.5t

Table 10

Distribution parameters in the proposed predictive model for welded stainless steel I-sections

Alloy	$\sigma_{ft}=\sigma_{wt}$	$\sigma_{fc}=\sigma_{wc}$	a	b	c	d
Austenitic	$0.8\sigma_{0.2}$	From Eq. (3)	$0.225b_f$	$0.05b_f$	$0.025h_w$	$0.225h_w$
Duplex, Ferritic	$0.6\sigma_{0.2}$	From Eq. (3)				

Table 11

Distribution parameters in the proposed predictive model for welded stainless steel box sections

Alloy	Ratio	$\sigma_{sft}=\sigma_{swt}$	e	f	g	h
Austenitic	$h/t(b_f/t)$<20	$0.8\sigma_{0.2}$	0	$5t_f$	0	$5t_w$
	$h/t(b_f/t)\geq$20	$0.8\sigma_{0.2}$	$t_w+0.025c_f$	$5t_f$	$0.025h_w$	$5t_w$
Duplex, Ferritic	$h/t(b_f/t)$<20	$0.6\sigma_{0.2}$	0	$5t_f$	0	$5t_w$
	$h/t(b_f/t)\geq$20	$0.6\sigma_{0.2}$	$t_w+0.025c_f$	$5t_f$	$0.025h_w$	$5t_w$

Table 12

Summary of residual stress prediction ratios (Predicted/Test)

Source	Test data from this study				Lagerqvist and Olsson [14]		Wang et al. [15]	Bredenkamp et al. [13]
Section	I-section		Box section		I-section		I-section	I-section
Grade	Austenitic EN 1.4301	Duplex EN 1.4462	Austenitic EN 1.4301	Duplex EN 1.4462	Austenitic EN 1.4301	Duplex EN 1.4462	Austenitic EN 1.4401	Ferritic EN 1.4003
Mean	1.05	0.96	0.99	1.02	0.96	1.59	0.97	1.32
COV	0.71	0.68	0.58	0.59	0.41	0.38	1.00	1.04